Journal of Alloys and Compounds 504 (2010) 70–75

Contents lists available at ScienceDirect

Journal of Alloys and Compounds

journal homepage: www.elsevier.com/locate/jallcom

Study of formation mechanism of barium hexaferrite by sintering curve

H.Z. Wang[a], Q. He[a], G.H. Wen[a], F. Wang[a], Z.H. Ding[a], B. Yao[a,b,*]

[a] State Key Laboratory of Superhard Materials and Department of Physics, Jilin University, Changchun 130023, People's Republic of China
[b] Changchun Institute of Optics, Fine Mechanics and Physics, Chinese Academy of Sciences, Changchun 130021, People's Republic of China

ARTICLE INFO

Article history:
Received 3 March 2010
Received in revised form 5 May 2010
Accepted 5 May 2010
Available online 21 May 2010

Keywords:
Barium hexaferrite
Ball milling
Sintering shrinkage curve
Magnetic properties

ABSTRACT

Barium hexaferrite ($BaFe_{12}O_{19}$) with hexagonal structure was fabricated by sintering the mixture of α-Fe_2O_3 and $BaCO_3$, ball milling of the mixture followed by heat treatment as well as glycin–nitrate method and subsequent heat treatment, respectively. The mechanism of formation of the $BaFe_{12}O_{19}$ in the three kinds of procedures was investigated by using sintering shrinkage curve and XRD measurements. It was found that the α-Fe_2O_3 reacted with $BaCO_3$ to form $BaFe_2O_4$ with orthorhombic structure as the mixture were sintered above 660 °C firstly and then the $BaFe_2O_4$ reacted with α-Fe_2O_3 to form $BaFe_{12}O_{19}$ in a sintering temperature ranging from 770 to 920 °C. However, the α-Fe_2O_3 reacted with $BaCO_3$ to form $Ba_xFe_{3-x}O_4$ with spinel structure when the mixture was milled for 80 h, while the $BaFe_{12}O_{19}$ was obtained by annealing the $Ba_xFe_{3-x}O_4$ at 700–1000 °C. In the glycin–nitrate procedure, the precursor powders containing α-Fe_2O_3, Fe_3O_4 and $BaFe_2O_4$ were fabricated by self-propagating reaction firstly, and then the single $BaFe_{12}O_{19}$ was produced by sintering the precursor powders at 1000 °C. The magnetic properties of the $BaFe_{12}O_{19}$ produced by the three kinds of procedures were reached. The saturation magnetization and the coercivity of the $BaFe_{12}O_{19}$ fabricated by ball milling followed by heat treatment were 47.24 emu/g and 5086.34 Oe, respectively, which were much larger than those of the $BaFe_{12}O_{19}$ produced by other procedures. The mechanism leading to that the $BaFe_{12}O_{19}$ produced by the different methods had different magnetic properties was discussed in the present work.

1. Introduction

M-type barium hexaferrite with hexagonal molecular structure is of great importance for perpendicular magnetic materials, due to that the raw material for barium hexaferrite is abundant, the manufacturing cost is low, its properties are stable and the problem of oxidation of the product is avoided [1–2]. Furthermore, the barium hexaferrite makes it potentially important in high-density perpendicular recording media, electromagnetic interference, magnetic fluids, microwave devices, etc. [1,3–7]. Specially, the properties in demagnetizing behavior, moderate coercivity, very low switching field distribution (SFD) and so on make the barium hexaferrite suitable for recording media [8–10].

The magnetic properties of barium hexaferrite originate from the Fe^{3+} ions of the barium hexaferrite structure. So people are interested in cationic substitution of Fe^{3+} ions, which causes the significant change of saturation magnetization and coercivity. For example, high anisotropic field of barium hexaferrite can be reduced by substitution of some ions, such as Co^{2+}, Zr^{4+}, Ni^{2+}, Ti^{4+}, Sn^{2+} and so on [11–15], for Fe^{3+}. However, these substitutions can cause the intrinsic coercivity to decrease effectively but at the expense of decrease in saturation magnetization. Therefore, the cationic substitutions are not a suitable way to alter the magnetic properties of barium hexaferrite. And then, people pay more attention to purity, grain size and morphology of the precursor powder [1,16]. In addition, in order to obtain the $BaFe_{12}O_{19}$ with fine grain and morphology of the precursor powder, many methods are suggested to produce barium hexaferrite, such as, conventional sinter route [1], sol–gel auto-combustion [17], chemical co-precipitation [18], salt-melt [19], low temperature combustion [20], mechanochemical processing [21], mechanical alloying [22], etc. In these methods procedure, the formation of barium hexaferrite all undergoes the intermediate phase. Whereas the intermediate phase transformation is often overlooked in the formation of barium hexaferrite process. In fact, the different intermediate phase transformation will have a great impact on the magnetic properties of barium hexaferrite during the formation of barium hexaferrite.

The conventional sinter method, mechanical alloy method and glycin–nitrate method are three common methods of preparing barium hexaferrite. In this work, the three methods are used to synthesize barium hexaferrite. The purpose is to reveal that the intermediate phase transformation of three kinds of procedures are different in the formation of barium hexaferrite process and the dif-

* Corresponding author at: State Key Laboratory of Superhard Materials and Department of Physics, Jilin University, Changchun 130023, People's Republic of China. Tel.: +86 43186176355.
E-mail address: binyao@jlu.edu.cn (B. Yao).

0925-8388/$ – see front matter.
doi:10.1016/j.jallcom.2010.05.050

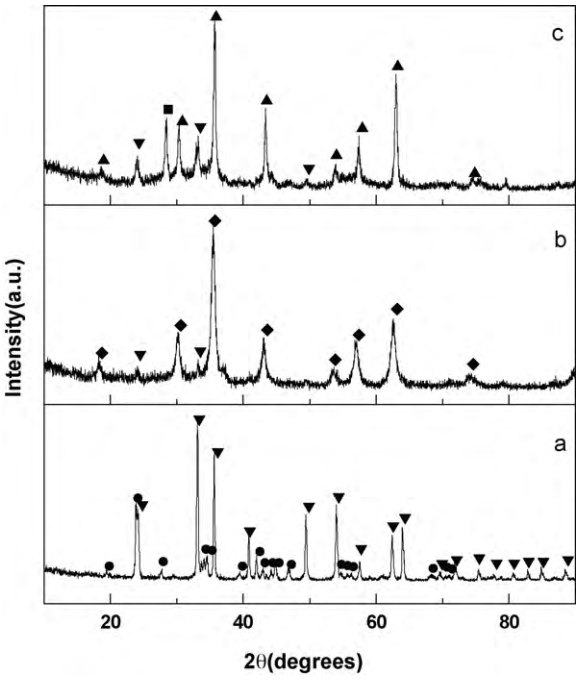

Fig. 1. XRD patterns for conventional route (a), 80 h high-energy ball-milled $BaCO_3 + 6F_2O_3$ (b) and glycin–nitrate method (c) powders: (▼) α-Fe_2O_3; (●) $BaCO_3$; (♦) $Ba_xFe_{3-x}O_4$; (■) $BaFe_2O_4$; (▲) Fe_3O_4.

ferent phase transformation have a great influence on the magnetic properties of barium hexaferrite in the aspects of physics method and chemical method, equilibrium condition and non-equilibrium condition.

2. Experimental procedures

A mixture of 99% pure nonmagnetic α-Fe_2O_3 and $BaCO_3$ powders were used as starting materials for production of $BaFe_{12}O_{19}$ by conventional sinter method and mechanochemical reaction in a high-energy ball milling. The molar ratio of α-Fe_2O_3 to $BaCO_3$ was 6:1 in the mixture. In the conventional sinter process, the mixture was sintered from room temperature to 1000 °C. In the mechanochemical reaction process, the mixture was milled in a mill firstly and annealed under ambient pressure in a temperature ranging from room temperature to 1000 °C. A stainless vial filled with stainless balls having diameter of 5–15 mm was used as the milling medium. The mass of the mixture was 7 g and the balls-to-powder mass ratio was 15:1. The mixture was milled under air ambient without any additives (dry milling). In the glycin–nitrate process, the starting materials used were 99% pure iron nitrate($Fe(NO_3)_3{\cdot}9H_2O$), barium nitrate($Ba(NO_3)_2$), glycin and distilled water. Appropriate amount of $Fe(NO_3)_3{\cdot}9H_2O$ and $Ba(NO_3)_2$, in a Fe/Ba molar ratio of 12 were dissolved in the required amount of distilled water. The molar ratio of glycin to total moles of nitrate ions was adjusted at 1.5:1. The precursor powders were annealed under ordinary pressure ambient in a temperature ranging from room temperature to 1000 °C. These samples were pressed into disk (under pressure of 0.2 GPa) and sintered for 2 h in air atmosphere in a temperature ranging from 700 to 1000 °C.

The structure of the samples was characterized by using a Rigaku-D-Max X-ray diffractometer (XRD) with CuKα radiation (λ = 1.5418 Å). The sintering shrinkage curve was measured using a Netzsch DIL 402C dilatometer, which was operated from room temperature to 1000 °C with an air purge flow rate of 60 ml/min. The thermal behaviors of the samples were examined by thermogravimetric and differential scanning calorimeter (TG/DTA, STA 449C, Netzsch) in a temperature ranging from room temperature up to 1000 °C with a heating rate of 10 °C/min. Raman spectra of the samples were recorded at room temperature, using a Renishaw inVia Raman spectrometer with a charge coupled device detector. An argon-ion laser (514.5 nm wavelength) was used as the excimer. The laser power operated on the sample was 20 mW. Measurement of magnetic properties were performed in a vibrating sample magnetometer (VSM) at room temperature with a maximum applied field of 1100 kA/m (Lake Shore 7410 vibrating sample magnetometer).

3. Results and discussion

Fig. 1(a) shows the XRD pattern of the mixture of α-Fe_2O_3 and $BaCO_3$ powders with molar ratio of 6:1, indicating that the mixture consists of α-Fe_2O_3 and $BaCO_3$ with rhombohedra and orthorhombic structure, respectively. Using the mixture as starting material, we try to fabricate barium hexaferrite ($BaFe_{12}O_{19}$) by conventional sinter method. In order to understand the mechanism of formation of the $BaFe_{12}O_{19}$, a sintering shrinkage curve for the cylinder of the mixture is measured in a temperature ranging from room temperature to 1000 °C, as shown in solid line in Fig. 2(a). In order to better understand the sintering reaction process of the mixture by the sintering shrinkage curve, the curve is differentiated, and the differential result is also shown by dot line in Fig. 2(a). As AB segment of the curve in Fig. 2(a) shows, the length variation fraction of the mixture ΔL ($\Delta L = (L - L_0)/L_0$, here L and L_0 are lengths of the cylinder of the mixture at a temperature (T) and room temperature (T_0), respectively) which increases linearly with increasing temperature in a temperature ranging from room temperature to 660 °C, because of the thermal expansion of the mixture. When the temperature exceeds 660 °C, the ΔL begins to decrease non-linearly till the temperature up to about 920 °C, as shown in BCD segment of the curve, implying that a chemical reaction may occur. This reaction is confirmed by thermal gravity measurement, as shown in Fig. 3(a). It can be seen from Fig. 3(a) that the mass of the mixture decreases slowly with increasing temperature between room temperature and 660 °C, but greatly in a temperature ranging from 660 to 920 °C. The former is due to the release of gas and vapor absorbed on the surface of the mixture, and the latter implies the release of some gas produced by some chemical reaction. Some literatures reported previously [23] that α-Fe_2O_3 reacts with $BaCO_3$ to form $BaFe_2O_4$ with orthorhombic structure as they are sintered above 600 °C in air ambient, accompanied by release of CO_2. The reaction can be expressed as follow:

$$BaCO_3 + Fe_2O_3 \rightarrow BaFe_2O_4 + CO_2\uparrow \quad (1)$$

Therefore, we deduce that the α-Fe_2O_3 reacts with $BaCO_3$ to form $BaFe_2O_4$ with orthorhombic structure as they are sintered above 660 °C.

In order to demonstrate this reaction, the mixture is sintered for 2 h at 700 °C in air ambient. Fig. 4(a) shows the XRD pattern of the sintered mixture. It is found that the intensity of diffraction peaks of $BaCO_3$ decreases greatly, meanwhile, some additional diffraction peaks are observed in the XRD profile besides the diffraction peaks of α-Fe_2O_3. These additional peaks are demonstrated to be the diffractions of $BaFe_2O_4$ with orthorhombic structure. This implies that the α-Fe_2O_3 reacts with $BaCO_3$ to form $BaFe_2O_4$ with orthorhombic structure as they are sintered at 700 °C in air ambient.

The dot line in Fig. 2(a) indicates the that variation rate of length variation fraction with temperature changing in BC segment is much smaller than that in CD segment, which implies that some additional chemical reaction may occur in CD segment besides the reaction between α-Fe_2O_3 and $BaCO_3$. In order to understand the additional reaction, the mixture is sintered for 2 h at 1000 °C, and measured by XRD, as shown in Fig. 5(a). In comparison with Fig. 4(a), the intensity of diffraction peak of the α-Fe_2O_3 decreases greatly and the diffraction peak of the $BaFe_2O_4$ is not almost observed in Fig. 5(a), meanwhile, the diffraction peaks of barium hexaferrite ($BaFe_{12}O_{19}$) are observed and become dominant, while the diffraction peaks of the α-Fe_2O_3 become very weak. The results of Fig. 4(a) and Fig. 5(a) indicate that the mixture sintered at 1000 °C mainly consists of $BaFe_{12}O_{19}$ and a small amount of α-Fe_2O_3. The $BaFe_{12}O_{19}$ is formed by following reaction process:

$$BaFe_2O_4 + 5Fe_2O_3 \rightarrow BaFe_{12}O_{19} \quad (2)$$

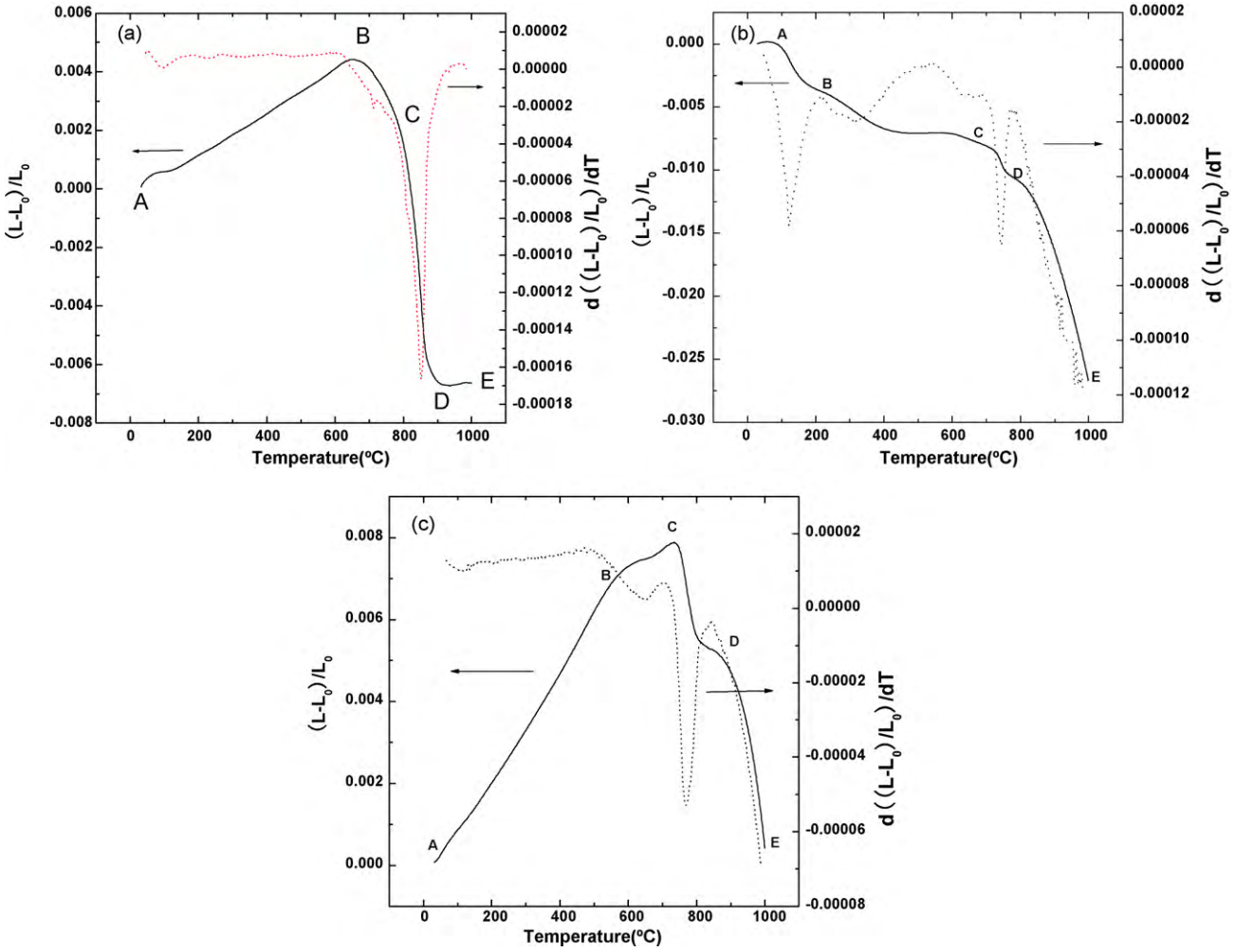

Fig. 2. The sintering shrinkage curves of three samples: solid line shows the sintering shrinkage curve; dot line shows differential line of sintering shrinkage curve samples: conventional route (a), mechanical alloying (b) and glycin–nitrate method (c).

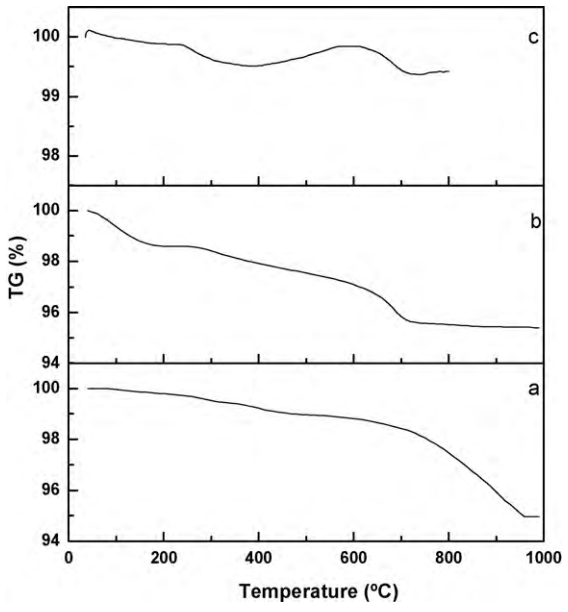

Fig. 3. TG curves of precursor powders which were prepared by conventional route (a), mechanical alloying (b) and glycin–nitrate method (c) in air.

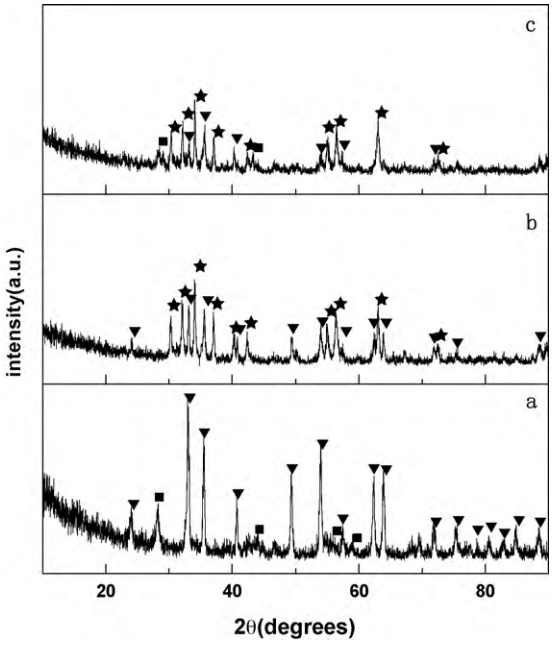

Fig. 4. The XRD diffraction patterns of precursor powders which were prepared by conventional route (a), mechanical alloying (b) and glycin–nitrate method (c) sintered for 2 h at 700 °C: (▼) α-Fe_2O_3; (■) $BaFe_2O_4$; (★) $BaFe_{12}O_{19}$.

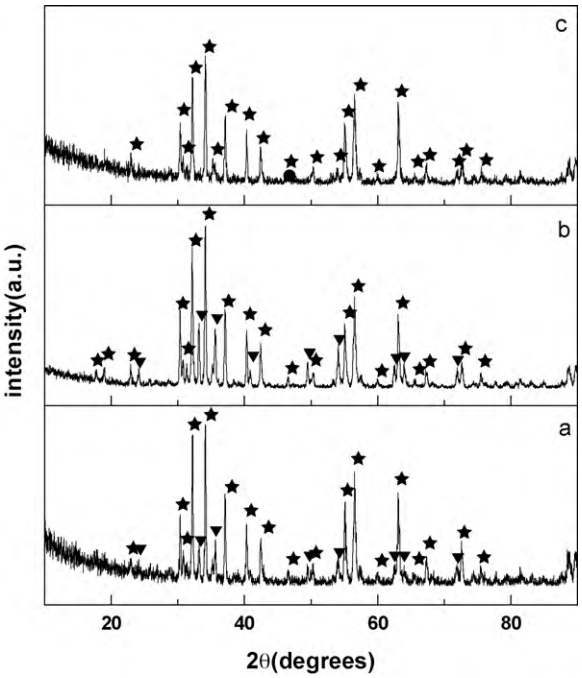

Fig. 5. The XRD diffraction patterns of $BaFe_{12}O_{19}$ prepared by conventional route (a), mechanical alloying (b) and glycin–nitrate method (c) for 2 h at 1000 °C: (▼) α-Fe_2O_3; (★) $BaFe_{12}O_{19}$.

Since the density of $BaFe_{12}O_{19}$ is larger than that of $BaFe_2O_4$ and α-Fe_2O_3, the formation of the $BaFe_{12}O_{19}$ results in a decrease in length, in agreement with the result indicated by dot line in Fig. 2(a). Based on the above discussion, the formation of the $BaFe_{12}O_{19}$ can be deduced as follows: firstly, the α-Fe_2O_3 reacts with $BaCO_3$ to form $BaFe_2O_4$ phase when the sintering temperature is above 660 °C, and then the $BaFe_2O_4$ begins to react with α-Fe_2O_3 to form $BaFe_{12}O_{19}$ as the sintering temperature is higher than 770 °C, this reaction completes at about 920 °C. Since no reaction occurs above 920 °C, the length variation fraction also does not change, as shown in DE segment in Fig. 2(a).

The mixture of the $BaCO_3$ and α-Fe_2O_3 powders as the starting materials is milled for 80 h. Expressly after ball milling for 80 h, the mixture is completely different from the starting materials, the color of mixture changes slowly from red to black. Fig. 1(b) shows the XRD diffraction pattern of the mixture milled for 80 h, indicating that the diffraction peaks of the $BaCO_3$ disappear completely and the peaks of the α-Fe_2O_3 almost disappear, while some strong diffraction peaks belonging to the $Ba_xFe_{3-x}O_4$ with spinel structure is observed. That implies that some α-Fe_2O_3 react with $BaCO_3$ to form $Ba_xFe_{3-x}O_4$ with spinel structure, in agreement with the results reported by He et al. [24]. The 80 h-milled mixture consists of the $Ba_xFe_{3-x}O_4$ and a small amount of α-Fe_2O_3.

Now we try to fabricate the barium hexaferrite ($BaFe_{12}O_{19}$) by sintering the 80 h-milled mixture. In order to understand the mechanism of formation of the $BaFe_{12}O_{19}$ in the sintering process, a sintering shrinkage curve for the 80 h-milled mixture is measured in a temperature ranging from room temperature to 1000 °C, as shown in solid line in Fig. 2(b). In order to better understand the sintering reaction process of the 80 h-milled mixture by the sintering shrinkage curve, the curve is differentiated, and the differential result is also shown by dot line in Fig. 2(b). Being different from the sintering curve (a), the sintering curve (b) keeps on shrinking in the whole temperature coverage. As ABC segment of the curve in Fig. 2(b) shows, the length variation fraction of the 80 h-milled mixture ΔL decreases sharply with increasing temperature in a temperature ranging from room temperature to around 110 °C and then slowly in the temperatures between 110 and 700 °C. The contraction in AB segment is due to the evaporation of adsorbed vapor, while the contraction in BC segment is attributed to the evaporation of absorbed gases. When the temperature exceeds 700 °C, the ΔL begins to decrease quickly till the temperature up to 1000 °C, as shown in CDE segment of the curve, implying that a chemical reaction may occur. This reaction is confirmed by thermal gravity measurement, as shown in Fig. 3(b). In the TG profiles, a weight loss in a temperature ranging from room temperature to 700 °C is observed in the TG curve, which confirms the former interpretation. But a great weight loss occurs in a temperature rang from 650 to 720 °C, supposing that the weight loss may be mainly associated with the Ba^{2+} occupying the lattice oxygen in the process of the formation of barium hexaferrite, which result in the release of the oxygen. In order to understand this reaction, the 80 h-milled mixture is pressed into disk and sintered for 2 h at 700 °C in air ambient. Fig. 4(b) shows the XRD diffraction patterns of the 80 h-milled mixture sintered. It is found that the diffraction peaks of $Ba_xFe_{3-x}O_4$ disappear completely, while the diffraction peaks of α-Fe_2O_3 and $BaFe_{12}O_{19}$ phases are observed, indicating that the $Ba_xFe_{3-x}O_4$ phase transforms into $BaFe_{12}O_{19}$ and α-Fe_2O_3 phases.

The dot line in Fig. 2(b) indicates that variation rate of the ΔL with temperature has obvious change in CD segment of the sintering curve, which implies that a chemical reaction may occur in the segment. In order to further understand the chemical reaction, the 80 h-milled mixture is sintered for 2 h at 1000 °C in air ambient, and the XRD pattern of this sample is shown in Fig. 5(b). In comparison with Fig. 4(b), the intensity of diffraction peaks of $BaFe_{12}O_{19}$ increases greatly and the diffraction peaks of α-Fe_2O_3 decrease, no diffraction peak of other phase can be observed. We suppose that the chemical reaction can be expressed as follows:

$$Ba_xFe_{3-x}O_4 \rightarrow BaFe_{12}O_{19} + O_2\uparrow \quad (3)$$

Since the density of $BaFe_{12}O_{19}$ is larger than that of $Ba_xFe_{3-x}O_4$ and α-Fe_2O_3, the formation of the $BaFe_{12}O_{19}$ results in the decrease in volume, in agreement with the result indicated by dot line in Fig. 2(b). In addition, the release of the O_2 leads to decrease in weight, in agreement with the TG curve of weight loss in Fig. 3(b). Based on the above discussion, the formation of $BaFe_{12}O_{19}$ can be deduced as follows: Firstly, the $Ba_xFe_{3-x}O_4$ is fabricated by mechanochemical reaction of α-Fe_2O_3 and $BaCO_3$, and then the $Ba_xFe_{3-x}O_4$ transforms into $BaFe_{12}O_{19}$ phase when it is sintered at the temperatures of 700–780 °C. With increasing temperature, the content of α-Fe_2O_3 decreases gradually, the content of the $BaFe_{12}O_{19}$ turns to be much more and compacter so that the sintering curve decreases from the beginning of 780 up to 1000 °C, so the length variation fraction continues to decrease, as shown in DE segment in Fig. 2(b).

We also tried to fabricate $BaFe_{12}O_{19}$ by using the glycin–nitrate technique. We firstly fabricate the precursor powders by self-propagating reaction of the mixture of iron nitrate, barium nitrate and glycin, and then prepare $BaFe_{12}O_{19}$ by sintering the precursor powders. Fig. 1(c) shows the XRD pattern of the precursor powders, indicating that the precursor powders consist of α-Fe_2O_3, Fe_3O_4 and $BaFe_2O_4$. In order to understand the mechanism of formation of $BaFe_{12}O_{19}$, a sintering shrinkage curve is measured for the precursor powders in a temperature ranging from room temperature to 1000 °C, as shown in solid line in Fig. 2(c). In order to better understand the sintering reaction process of the mixture by the sintering shrinkage curve, the curve is differentiated, and the differential result is shown by dot line in Fig. 2(c). Being similar to the sintering curve in Fig. 2(a), the length variation fraction of the precursor powders ΔL also increases linearly with increasing temperature in a temperature ranging from room temperature to 710 °C, as shown in ABC segment of the curve in Fig. 2(c), which is due to the thermal expansion of the precursor powders. But the

Table 1
Magnetic properties of $BaFe_{12}O_{19}$ by sintering three starting materials.

Sample no.	H_C (Oe)	M_S (emu/g)	M_r (emu/g)
A	2634.94	60.73	32.36
B	5086.37	47.24	26.38
C	4012.13	60.37	31.13

length variation fraction of the precursor powders ΔL increases slowly with increasing temperature in BC segment of the curve, it can be interpreted that a little glycin volatilize from the precursor powders. When the temperature exceeds 710 °C, the ΔL begins to decrease non-linearly with increasing temperature up to about 1000 °C, as shown in CDE segment of the curve, implying that a chemical reaction may occur. This reaction is confirmed by thermal gravity measurement, as shown in Fig. 3(c). It can be seen from Fig. 3(c) that the weight of the precursor powders decreases slowly in the whole temperature coverage, but two obvious weight losses occur in a temperature ranging from 300 to 750 °C. The former is due to the release of gases which are produced by glycin combustion; and the latter is due to the chemical reaction of formation of $BaFe_{12}O_{19}$. Because the precursor powders contain α-Fe_2O_3 and $BaFe_2O_4$, the chemical reaction between them will be carried out following equation (2). In order to demonstrate this reaction, the precursor powders are sintered for 2 h at 700 °C in air ambient. Fig. 4(c) shows the XRD pattern of the sintered precursor powders. It is found that the intensity of diffraction peaks of $BaFe_2O_4$ and Fe_3O_4 decreases greatly, and some additional diffraction peaks are observed in the XRD profile besides diffraction peaks of α-Fe_2O_3. These additional peaks are demonstrated to be the diffractions of $BaFe_{12}O_{19}$. It implies that the α-Fe_2O_3 reacts with $BaFe_2O_4$ to form $BaFe_{12}O_{19}$ as they are sintered at 700 °C in air ambient.

The dot line in Fig. 2(c) indicates that variation rate of length variation fraction has obvious change in BCD segment of curve, which confirms that the chemical reaction occurs in CD segment. In order to better understand the chemical reaction, the precursor powders are sintered for 2 h at 1000 °C, its XRD pattern is shown in Fig. 5(c). In comparison with Fig. 4(c), the intensity of diffraction peaks of the α-Fe_2O_3 completely disappears, meanwhile, only the diffraction peaks of $BaFe_{12}O_{19}$ are observed. The result shows that the content of α-Fe_2O_3 continues to reduce in a temperature ranging from 710 to 1000 °C, resulting in the decrease in length, as shown in DE segment of curve in Fig. 2(c), in agreement with the result indicated by dot line in Fig. 2(c). Based on the above discussion, the formation of the $BaFe_{12}O_{19}$ can be deduced as follows: Firstly, iron nitrate, barium nitrate and glycin is used as raw materials to produce the precursor containing α-Fe_2O_3, Fe_3O_4 and $BaFe_2O_4$ by self-propagating reaction. Secondly, the precursor powders are sintered to fabricate $BaFe_{12}O_{19}$, and formed single barium hexaferrite at 1000 °C.

The hysteresis loop of three selected samples which are fabricated by sintering the mixture of α-Fe_2O_3 and $BaCO_3$, the 80 h-milled mixture and the precursor powders for 2 h at 1000 °C, are shown in Fig. 6 (denoted as sample A, sample B and sample C). From the VSM experiments, the magnetic parameters such as saturation magnetization (M_S), coercivity (H_C) and remnant magnetization (M_r), which are given in Table 1.

From Table 1, it is clearly seen that the value of saturation magnetization and remnant magnetization of $BaFe_{12}O_{19}$ fabricated by sintering 80 h-milled mixture is much lower than that of the $BaFe_{12}O_{19}$ produced by two other techniques; however, its coercivity is much larger than theirs. Moreover, the coercivity of $BaFe_{12}O_{19}$ fabricated by sintering 80 h-milled mixture is better than the coercivity of $BaFe_{12}O_{19}$ in the literature reported previously [1]. Generally, the coercivity of $BaFe_{12}O_{19}$ is related to purity, grain size, pinning and so on. The apparent grain size of samples

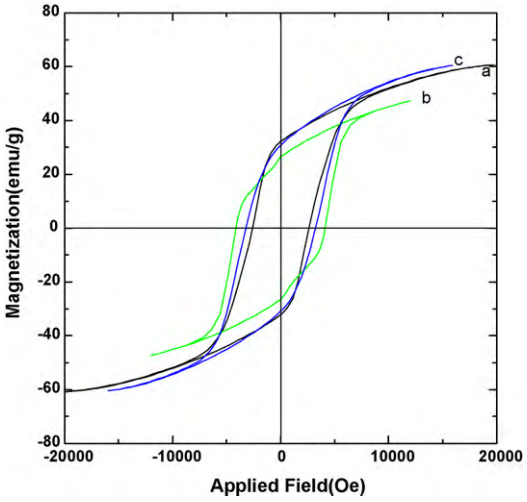

Fig. 6. Hysteresis loops of the precursor powders which were prepared by conventional route (a), mechanical alloying (b) and glycin–nitrate method (c) sintered for 2 h at 1000 °C.

is estimated by analyzing the X-ray diffraction peak broadening, using Scherrer's equation: $\langle D\rangle = 0.89\lambda/\beta_{1/2}\cos\theta$, here $\langle D\rangle$ is the average particle size, λ is the wavelength of the incident X-ray, θ is the corresponding Bragg angle and $\beta_{1/2}$ is the full-width at half-maximum (FWHM) of the XRD peak. The values of the average grain size of three samples, which are fabricated by sintering the mixture of α-Fe_2O_3 and $BaCO_3$, the 80 h-milled mixture and the precursor powders for 2 h at 1000 °C, are 31.0, 31.1 and 31.9 nm, respectively. The result shows that the grain sizes of $BaFe_{12}O_{19}$ prepared by the three techniques are similar to each other, indicating that the grain size is not the major influencing factor of the different coercivity of barium hexaferrite. As can be seen from Fig. 5, in the same sintering conditions (2 h at 1000 °C), the sample produced by glycin–nitrate procedure consists of single $BaFe_{12}O_{19}$ phase, while the samples produced by other two procedures consist of $BaFe_{12}O_{19}$ and a small amount of α-Fe_2O_3. However, the coercivity of $BaFe_{12}O_{19}$ fabricated by sintering 80 h-milled mixture is larger than the coercivity of $BaFe_{12}O_{19}$ fabricated by sintering the precursor powders. The result shows that the purity also is not the major influencing factor of the different coercivity of $BaFe_{12}O_{19}$. Because of there is a small amount of α-Fe_2O_3 in the $BaFe_{12}O_{19}$ fabricated by sintering 80 h-milled mixture, the pinning of effect of α-Fe_2O_3 is considered carefully. However, the $BaFe_{12}O_{19}$ which is fabricated by sintering the mixture of α-Fe_2O_3 and $BaCO_3$ also contains a small amount of α-Fe_2O_3, its coercivity is much smaller than that of the $BaFe_{12}O_{19}$ produced by other two techniques. The result shows that the pinning of effect of α-Fe_2O_3 is also not the major influencing factor of the different coercivity of $BaFe_{12}O_{19}$.

The Raman spectra of the $BaFe_{12}O_{19}$ prepared by sintering the mixture of α-Fe_2O_3 and $BaCO_3$, the 80 h-milled mixture and the precursor powders for 2 h at 1000 °C are shown at line a, b and c in Fig. 7. They show similar band structure. However, it is noted that relative intensity of the 284 cm^{-1} band of the $BaFe_{12}O_{19}$ prepared by sintering 80 h-milled mixture is much stronger than that of the $BaFe_{12}O_{19}$ prepared by two others. As we are known, the band at 284 cm^{-1} is attributed to the vibration of Fe–O bond, where the Fe^{3+} locates at the octahedral 2a site [25,26]. Therefore, the difference in the relative intensity implies that the atom species at the 2a site in the $BaFe_{12}O_{19}$ prepared by sintering 80 h-milled mixture may be different from that in the $BaFe_{12}O_{19}$ prepared by the two others. In the conventional sintering and glycin–nitrate procedures $BaFe_2O_4$ reacts with α-Fe_2O_3 to form $BaFe_{12}O_{19}$, where all of octahedral 2a sites are occupied by Fe^{3+} ions. However, since

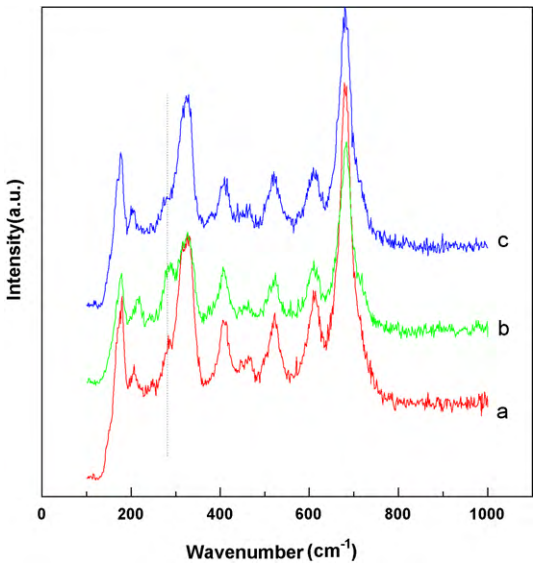

Fig. 7. The Raman spectra of $BaFe_{12}O_{19}$ prepared by sintering the mixture of α-Fe_2O_3 and $BaCO_3$ (line a), the 80 h-milled mixture (line b) and the precursor powders (line c) for 2 h at 1000 °C.

the Ba ions substitute for Fe ions at the octahedral 2a sites in the spinel type $Ba_xFe_{3-x}O_4$, they are all not move to O^{2-} sites of the $BaFe_{12}O_{19}$ but some of them still remain in the octahedral 2a sites when the $Ba_xFe_{3-x}O_4$ is annealed for preparation of the $BaFe_{12}O_{19}$. That leads to that some of the 2a sites are occupied by Ba^{2+} ions, and the other are occupied by Fe^{3+} ions in the $BaFe_{12}O_{19}$. Due to that some of the Fe^{3+} ions with spinning upward at the 2a sites are substituted by nonmagnetic Ba^{2+} ions in the $BaFe_{12}O_{19}$ prepared by annealing the $Ba_xFe_{3-x}O_4$, the net magnetic moment of the $BaFe_{12}O_{19}$ will decrease and the anisotropy will increase, leading to significant reduction in saturation magnetization and increase in coercivity. This result is in agreement with the results mentioned above. Besides, the ball milling process is a non-equilibrium process, the ball milling process creates defects which lead to the amorphization of the crystal structure, and improvement of the magnetic properties after annealing is due to the release of stress and the recovery from the defective structure, in agreement with the results of some literatures reported previously [27].

4. Conclusions

$BaFe_{12}O_{19}$ is fabricated by three kinds of procedures, respectively: (1) sintering mixture of α-Fe_2O_3 and $BaCO_3$, (2) ball milling of the mixture followed by heat treatment, and (3) glycin–nitrate method and subsequent heat treatment. The formation mechanism of the $BaFe_{12}O_{19}$ is different in the three kinds of procedures. In the first procedure, the α-Fe_2O_3 reacts with $BaCO_3$ to form an intermediate phase of $BaFe_2O_4$ firstly, and then the $BaFe_2O_4$ reacts with α-Fe_2O_3 to form $BaFe_{12}O_{19}$ in a sintering temperature ranging from 770 to 920 °C. In the second procedure, the α-Fe_2O_3 reacted with $BaCO_3$ to form $Ba_xFe_{3-x}O_4$ with spinel structure when the mixture were milled for 80 h, the $BaFe_{12}O_{19}$ was obtained by annealing the $Ba_xFe_{3-x}O_4$ at 700–1000 °C. And in the last procedure, the precursor powders containing α-Fe_2O_3, Fe_3O_4 and $BaFe_2O_4$ were fabricated by self-propagating reaction firstly, and then the single phase of $BaFe_{12}O_{19}$ was produced by sintering the precursor powders at 1000 °C. The saturation magnetization and the coercivity of the $BaFe_{12}O_{19}$ fabricated by the second procedure were 47.24 emu/g and 5086.34 Oe, respectively. The coercivity of the $BaFe_{12}O_{19}$ fabricated by the second procedure is larger than that of the $BaFe_{12}O_{19}$ produced by other two procedures, which is not related to grain size and phase composition but should be due to remaining Ba^{2+} ions in the octahedral 2a site, leading to significant reduction in saturation magnetization and increase in coercivity.

Acknowledgements

This work is supported by the Key Project of National Natural Science Foundation of China under grant no. 50532050, the “973” program under grant no. 2006CB604906, the Innovation Project of Chinese Academy of Sciences, the National Natural Science Foundation of China under grant nos. 6077601, 60506014, 10674133, 60806002 and 10874178, National Fund for Fostering Talents of Basic Science under grant no. J0730311.

References

[1] P. Sharma, R.A. Rocha, S.N. de Medeiros, A. Paesano Jr., J. Alloys Compd. 443 (2007) 37–42.
[2] X.F. Yang, Q.L. Li, J.X. Zhao, B.D. Li, Y.F. Wang, J. Alloys Compd. 475 (2009) 312–315.
[3] J.X. Qiu, L.J. Lan, H. Zhang, M.Y. Gu, J. Alloys Compd. 453 (2008) 261–264.
[4] T.G. Carreno, M.P. Morales, C.J. Serna, Mater. Lett. 43 (2000) 97–101.
[5] L.X. Wang, Q.T. Zhang, J. Alloys Compd. 469 (2009) 251–257.
[6] J.X. Qiu, M.Y. Gu, J. Alloys Compd. 415 (2006) 209–212.
[7] P. Xu, X.J. Han, C. Wang, H.T. Zhao, W.J. Zhang, Mater. Chem. Phys. 108 (2008) 196–200.
[8] G. Benito, M.P. Morales, J. Requena, V. Raposo, M. Vázquez, J.S. Moya, J. Magn. Magn. Mater. 234 (2001) 65–72.
[9] D.E. Speliotes, IEEE Trans. Magn. 23 (1987) 3143–3145.
[10] H.J. Richter, IEEE Trans. Magn. 29 (1993) 2185–2201.
[11] A. Gruskova, J. Slama, R. Dosudil, D. Kevicka, V. Jancarik, I. Toth, J. Magn. Magn. Mater. 242–245 (2002) 423–425.
[12] S. Yong, I.B. Shum, J.C. Kim, J. Appl. Phys. 91 (2002) 8465–8467.
[13] G. Turrili, F. Licci, A. Paoluzi, T. Besagni, IEEE Trans. Magn. 24 (1998) 2146–2149.
[14] P.A. Marino-Castellanos, J.C. Somarriba-Jarque, J. Anglada-Rivera, Phys. B: Condens. Matter 362 (2005) 95–102.
[15] C. Singh, S. Bindra-Narang, I.S. Hudiara, Bai Yang, J. Alloys Compd. 464 (2008) 429–433.
[16] J. Ding, H. Yang, W.F. Miao, P.G. McCormick, R. Street, J. Alloys Compd. 221 (1995) 70–73.
[17] J.L. Liu, W. Zhang, C.J. Guo, Y.W. Zeng, J. Alloys Compd. 479 (2009) 863–869.
[18] C.S. Wang, X.W. Qi, L.T. Li, Mater. Sci. Eng. B 99 (2003) 270–273.
[19] H. Sözeri, J. Magn. Magn. Mater. 321 (2009) 2717–2722.
[20] J.G. Huang, H.R. Zhuang, W.L. Li, Mater. Res. Bull. 38 (2003) 149–159.
[21] J. Ding, T. Tsuzuki, P.G. McCormick, J. Magn. Magn. Mater. 177–181 (1998) 931–932.
[22] J. Ding, R. Street, H. Nishio, J. Magn. Magn. Mater. 164 (1996) 385–389.
[23] H.P. Steier, J. Requena, J.S. Moya, J. Mater. Res. 14 (1999) 3647–3652.
[24] Q. He, H.Z. Wang, G.H. Wen, Y. Sun, B. Yao, J. Alloys Compd. 486 (2009) 246–249.
[25] J. Kreisel, G. Lucazeau, H. Vincent, J. Raman Spectrosc. 30 (1999) 115–120.
[26] W.Y. Zhao, P. Wei, X.Y. Wu, W. Wang, Q.J. Zhang, J. Appl. Phys. 103 (2008) 063902.
[27] G. Mendoza-Suarez, J.A. Matutes-Aquino, J.I. Escalante-Garcia, H. Mancha-Molinar, D. Rios-Jara, K.K. Johal, J. Magn. Magn. Mater. 223 (2001) 55–62.